

Random-phase approximation study of collective excitations in the Bose-Fermi mixed condensate of alkali-metal gases

T. Sogo, T. Miyakawa, T. Suzuki, and H. Yabu

Department of Physics, Tokyo Metropolitan University, 1-1 Minami-Ohsawa, Hachioji, Tokyo 192-0397, Japan

(Received 24 February 2002; revised manuscript received 3 May 2002; published 30 July 2002)

We perform a random-phase approximation study of collective excitations in a Bose-Fermi mixed degenerate gas of alkali-metal atoms at $T=0$. The calculation is done by diagonalization in a model space composed of particle-hole type excitations from the ground state, the latter being obtained from the coupled Gross-Pitaevskii and Thomas-Fermi equations. We investigate strength distributions for different combinations of Bose and Fermi multipole (L) operators with $L=0,1,2,3$. Transition densities and dynamical structure factors are calculated for collective excitations. A comparison with the sum rule prediction for the collective frequency is given. The time dependent behavior of the system after an external impulse is studied.

DOI: 10.1103/PhysRevA.66.013618

PACS number(s): 03.75.Fi, 05.30.Fk

I. INTRODUCTION

Collective excitation is one of the most prominent phenomena in quantum many-body systems such as liquid helium, electron gases, nuclei, etc. In the recently developed Bose-Einstein condensates of trapped atomic gases [1,2], collective oscillations were the first of the dynamical phenomena discovered [3]. Collective oscillations are characterized by various quantum numbers related to, e.g., the shape of oscillation or internal degrees of freedom of the constituents such as spin, isospin, etc. The oscillation frequency, the damping width, etc., depend on the interparticle interaction of the constituents, and thus provide a clue to unravel the dynamical correlation of the many-body system.

The study of the properties of trapped neutral atoms has been extended to Fermi systems [4] where the occurrence of Fermi degeneracy was observed, and also to a mixture of Bose and Fermi particles. The latter system with condensed bosons and degenerate fermions was recently realized experimentally [5,6]. This system is one typical example in which particles obeying different statistics are intermingled. Theoretical studies of the Bose-Fermi mixed system of cold atomic gases have been done for static properties [7–12], for the phase diagram and phase separation [13–15], for the stability of the system [16,17], and for collective excitations [18–20].

In Ref. [18] the sum rule approach was applied for collective excitations in the Bose-Fermi mixed system. Average excitation energies for states with multipoles $L=0,1,2$ were calculated for both in-phase and out-of-phase modes of the Bose and Fermi particles, and the dependence on the Bose-Fermi interaction strength was studied. The sum rule approach is a powerful technique for collective states in quantum many-body systems, and has been successfully applied to the excitation of Bose condensed systems (see Refs. [2,21]). It does not, however, give direct information on the eigenstates of the system, but rather an average behavior of the strength distribution for the adopted multipole excitation operator. For a more detailed investigation of the dynamical properties of the system, one would need a study of individual eigenstates.

In the present paper we extend the previous study [18] of collective excitations in the Bose-Fermi mixed system. We calculate full particle-hole type excitations by diagonalization of a random-phase approximation type matrix. The motive of this calculation is threefold. First of all, the calculation allows us to study the excitation spectrum and the strength distribution, in contrast to the sum rule method, which focuses on the strength-weighted average of the prescribed multipole operators. We study, for instance, the degree of collectivity of the excitations depending on the strength of the boson-fermion interaction, and estimate the damping of the collective excitation albeit within the space of particle-hole excitations. Information on the wave function allows us to calculate observables such as the dynamical structure factor. The latter for Bose-condensed systems is now becoming available experimentally by two-photon spectroscopy [22] and is being studied theoretically [23]. Secondly, we compare the results with those obtained from the sum rule approach. This provides a check on the approximation adopted in the calculation such as the model space truncation. The comparison also allows one to examine the structure of the low- and high-lying collective modes which was speculated in [18] through the mixing angle θ of multipole operators. Third, we can predict the time-dependent behavior of the system for a given external perturbation. This process is actually the one that was employed in the previous experimental study of collective excitations in a Bose-Einstein condensate (BEC). A RPA study of the Bose-Fermi mixed system was recently done in [20], where the response for an external multipole field is formulated in the form of an integral equation. In the present calculation we approach the problem by diagonalizing the RPA matrix, by incorporating the discrete nature of the excitation in an isolated trapped system, and investigate, in particular, the properties of the strength distribution for a combination of Bose and Fermi operators and for various values of the Bose-Fermi interaction strengths.

The content of the paper is as follows. In the next section we derive the RPA equation for the Bose-Fermi mixed system using the equation of motion for particle-hole type excitation operators. The single-particle (hole) states are obtained in the mean-field calculation, i.e., by solving the coupled

Gross-Pitaevskii and Thomas-Fermi equations. In Sec. III we first briefly describe the parameters and the numerical procedure employed in the present calculation. We then turn to detailed studies of the results obtained, including ground state density, single-particle states, and strength distribution for each multipole. Comparison with the sum rule calculation is given. Transition densities and dynamical structure factors for some of the collective excitations are presented. We finally consider the time development of the system after an external multipole impulse on the system. The last section is devoted to summary and conclusions.

II. FORMULATION

We consider a dilute spin-polarized Bose-Fermi mixed system trapped in a spherically symmetric harmonic oscillator potential at $T=0$. The system is described by the Hamiltonian

$$\hat{H} = \hat{H}_0 + \hat{V}_b + \hat{V}_{bf}, \quad (1)$$

with

$$\begin{aligned} \hat{H}_0 = & \int d^3r \hat{\psi}^\dagger(\vec{r}) \left[-\frac{\hbar^2}{2m} \nabla^2 + \frac{1}{2} m \omega_0^2 r^2 \right] \hat{\psi}(\vec{r}) \\ & + \int d^3r \hat{\phi}^\dagger(\vec{r}) \left[-\frac{\hbar^2}{2m} \nabla^2 + \frac{1}{2} m \omega_0^2 r^2 \right] \hat{\phi}(\vec{r}), \\ \hat{V}_b = & \frac{1}{2} g \int \int d^3r d^3r' \hat{\phi}^\dagger(\vec{r}) \hat{\phi}^\dagger(\vec{r}') \delta^{(3)}(\vec{r} - \vec{r}') \hat{\phi}(\vec{r}') \hat{\phi}(\vec{r}), \\ \hat{V}_{bf} = & h \int \int d^3r d^3r' \hat{\phi}^\dagger(\vec{r}) \hat{\psi}^\dagger(\vec{r}') \delta^{(3)}(\vec{r} - \vec{r}') \hat{\psi}(\vec{r}') \hat{\phi}(\vec{r}), \end{aligned} \quad (2)$$

where $\hat{\phi}$ and $\hat{\psi}$ are the boson and fermion field operators. We take, for simplicity, the mass m and the trapping frequency ω_0 to be the same for the boson and the fermion. The boson-boson and boson-fermion interaction strengths for the pseudopotentials, g and h , are related to the s -wave scattering lengths a_{bb} and a_{bf} through $g = 4\pi\hbar^2 a_{bb}/m$, $h = 4\pi\hbar^2 a_{bf}/m$, while the fermion-fermion interaction is omitted as we consider a polarized dilute system at low temperature.

According to the Landau picture of a quantum liquid, low-lying excited states of the system may be described by quasiparticle excitations which have the structure of particle-hole (p - h) type excitations from the ground state. The small amplitude collective oscillations of the system, corresponding to zero sound, are given by the coherent superposition of these p - h excitations and are well described by the RPA for many fermion systems. The corresponding excitations in the Bose condensed system have been formulated in a Bogoliubov-de Gennes type equation. The latter is essentially the same as the one obtained in RPA, and we consider the two types of excitation on the same footing below.

In order to formulate the RPA for the Bose-Fermi mixed system, we first determine the ground state in the mean-field

approximation. The mean field obtained provides us with single-particle energies and wave functions. Let us expand the field operators in terms of a complete set of single-particle wave functions as

$$\hat{\phi}(\vec{r}) = \sum_k \phi_k(\vec{r}) b_k, \quad \hat{\psi}(\vec{r}) = \sum_\alpha \psi_\alpha(\vec{r}) a_\alpha, \quad (3)$$

where b_k and a_α are boson and the fermion annihilation operators in the single-particle states specified by the wave functions ϕ_k and ψ_α . They satisfy the standard commutation or anticommutation relations. The single-particle states with quantum numbers k or α are determined by minimizing the energy expectation value. The trial wave function of the system is given by the product of N_b bosons in a single state $\phi_{k=0}(\vec{r})$ and the Slater determinant of N_f different fermionic states $\psi_\alpha(\vec{r})$. From the stationary condition of energy for the variation of these wave functions with a given number of bosons N_b and fermions N_f , we obtain the set of coupled equations, i.e., the Gross-Pitaevskii equation for the boson wave function,

$$\begin{aligned} & \left[-\frac{\hbar^2}{2m} \nabla^2 + \frac{1}{2} m \omega_0^2 r^2 + g N_b |\phi_0(\vec{r})|^2 + h \rho_f(\vec{r}) \right] \phi_0(\vec{r}) \\ & = \mu_b \phi_0(\vec{r}), \end{aligned} \quad (4)$$

and the mean-field equation for the occupied fermion states

$$\begin{aligned} & \left[-\frac{\hbar^2}{2m} \nabla^2 + \frac{1}{2} m \omega_0^2 r^2 + h N_b |\phi_0(\vec{r})|^2 \right] \psi_\alpha(\vec{r}) \\ & = \epsilon_\alpha^f \psi_\alpha(\vec{r}), \end{aligned} \quad (5)$$

where

$$\rho_f(\vec{r}) = \sum_{\alpha}^{\text{occupied}} |\psi_\alpha(\vec{r})|^2 \quad (6)$$

is the ground state density of fermions, μ_b is the boson chemical potential, and ϵ_α^f are the single-particle energies for the fermion. The set of equations (4) and (5) together with the fermion number condition

$$\int d^3r \rho_f(\vec{r}) = N_f \quad (7)$$

constitute a closed set of equations. The single-particle wave functions are normalized to unity. In Eq. (4) we approximate the factor $N_b - 1$ by N_b . Once the single-particle wave functions for the occupied states are obtained from Eqs. (4) and (5), the wave functions of the unoccupied states are calculated from a similar set of equations, i.e.,

$$\begin{aligned} & \left[-\frac{\hbar^2}{2m} \nabla^2 + \frac{1}{2} m \omega_0^2 r^2 + g N_b |\phi_0(\vec{r})|^2 + h \rho_f(\vec{r}) \right] \phi_k(\vec{r}) \\ & = \epsilon_k^b \phi_k(\vec{r}) \end{aligned} \quad (8)$$

for bosons with $k \neq 0$, and the same Eq. (5) for fermions but for unoccupied states. Orthogonality of these wave functions to the occupied ones is automatically satisfied [24].

For a large number of particles with a smooth mean-field potential, the Thomas-Fermi calculation provides a good approximation. Assuming this to be the case, we determine the fermionic ground state density ρ_f by using

$$\frac{\hbar^2}{2m} [6\pi^2 \rho_f(\vec{r})]^{2/3} + \frac{1}{2} m \omega_0^2 r^2 + \hbar N_b |\phi_0(\vec{r})|^2 = \epsilon_F \quad (9)$$

together with Eq. (4) instead of fully solving the coupled set of equations (4) and (5). The Fermi energy ϵ_F is determined by integrating the density $\rho_f(\vec{r})$ so as to give the fermion number. The numerical consistency of this procedure will be shown in the next section. With ρ_f and ϕ_0 so determined, the wave functions ϕ_k ($k \neq 0$) and ψ_α are obtained as described above.

We assume below that the mean field is spherically symmetric, and the single-particle quantum numbers α and k involve standard radial and angular momentum quantum numbers (n, ℓ, m). (Note that the spin quantum number is frozen.) We consider the case in which the fermionic ground state (Slater determinant) is m -closed and thus is consistent with the spherically symmetric mean field. We denote by p (h) the fermion single-particle states unoccupied (occupied) in the Slater determinant, i.e., those above (below) the Fermi energy ϵ_F . For the bosons at $T=0$ the occupied state is the lowest single-particle state $k=0$.

We now define the creation and annihilation multipole operators of the excited state $|\nu LM\rangle$ with angular momentum quantum numbers L, M and an additional quantum number ν ,

$$Q_{\nu LM}^\dagger = F_{\nu LM}^\dagger + B_{\nu LM}^\dagger, \quad (10)$$

$$\begin{aligned} F_{\nu LM}^\dagger &= \sum_{ph} \sum_{m_p m_h} [X_{phL}^\nu \langle l_p m_p l_h - m_h | LM \rangle \\ &\times (-1)^{l_h - m_h} a_{p l_p m_p}^\dagger a_{h l_h m_h} - Y_{phL}^\nu \langle l_h m_h l_p - m_p | LM \rangle \\ &\times (-1)^{l_p - m_p} a_{h l_h m_h}^\dagger a_{p l_p m_p}], \end{aligned} \quad (11)$$

$$\begin{aligned} B_{\nu LM}^\dagger &= \frac{1}{\sqrt{N_b}} \sum_{k \neq 0} [U_{kL}^\nu b_{kLM}^\dagger b_0 \\ &- V_{kL}^\nu (-1)^{L+M} b_0^\dagger b_{kL-M}], \end{aligned} \quad (12)$$

where X, Y, U, V are the amplitudes to be determined in the RPA, and $\langle l_p m_p l_h - m_h | LM \rangle$ is the Clebsch-Gordan coefficient.

In the RPA the operator Q is determined so as to satisfy the equation of motion

$$[\hat{H}, Q_{\nu LM}^\dagger] \approx \hbar \Omega_\nu Q_{\nu LM}^\dagger, \quad (13)$$

where the terms on the left hand side (LHS) which involve different combinations of operators $a^\dagger, a, b^\dagger, b$ from that in Q^\dagger are neglected by the assumption of the RPA. The state

$$|\nu LM\rangle = Q_{\nu LM}^\dagger |0\rangle \quad \text{with} \quad Q_{\nu LM} |0\rangle = 0 \quad (14)$$

is then an approximate eigenstate of the Hamiltonian together with the correlated ground state given by $|0\rangle$. The amplitudes satisfy the orthonormality condition

$$\begin{aligned} \sum_{ph} (X_{phL}^{\nu*} X_{phL}^{\nu'} - Y_{phL}^{\nu*} Y_{phL}^{\nu'}) + \sum_{k \neq 0} (U_{kL}^{\nu*} U_{kL}^{\nu'} - V_{kL}^{\nu*} V_{kL}^{\nu'}) \\ = \delta_{\nu\nu'}. \end{aligned} \quad (15)$$

Substituting Eq. (10) into Eq. (13) we obtain the eigenvalue equation in matrix form:

$$\begin{pmatrix} A_{XX} & A_{XU} & B_{XY} & B_{XV} \\ A_{UX} & A_{UU} & B_{UY} & B_{UV} \\ -B_{XY} & -B_{XV} & -A_{XX} & -A_{XU} \\ -B_{UY} & -B_{UV} & -A_{UX} & -A_{UU} \end{pmatrix} \begin{pmatrix} X \\ U \\ Y \\ V \end{pmatrix} = \hbar \Omega_\nu \begin{pmatrix} X \\ U \\ Y \\ V \end{pmatrix}, \quad (16)$$

where the submatrices A and B are given by

$$\begin{aligned} (A_{XX})_{ph, p' h'} &= [\epsilon_{p l_p}^f - \epsilon_{h l_h}^f] \delta_{p, p'} \delta_{h, h'} \delta_{l_p, l'_p} \delta_{l_h, l'_h}, \\ (A_{XU})_{ph, k} &= \frac{h \sqrt{N_b}}{4\pi} \frac{\hat{l}_p \hat{l}_h}{\hat{L}} (-1)^{l_h} \langle l_p 0 l_h 0 | L 0 \rangle \\ &\times \int dr r^2 R_{p l_p}^f R_{h l_h}^f R_{k L}^b R_{00}^b, \\ (A_{UX})_{k, ph} &= (A_{XU})_{ph, k}, \\ (A_{UU})_{k, k'} &= [\epsilon_{k L}^b - \mu_b] \delta_{kk'} \\ &+ \frac{g N_b}{4\pi} \int dr r^2 R_{k L}^b R_{k' L}^b R_{00}^b R_{00}^b, \\ (B_{XY})_{ph, p' h'} &= 0, \\ (B_{XV})_{ph, k} &= \frac{h \sqrt{N_b}}{4\pi} \frac{\hat{l}_p \hat{l}_h}{\hat{L}} (-1)^{l_p} \langle l_p 0 l_h 0 | L 0 \rangle \\ &\times \int dr r^2 R_{p l_p}^f R_{h l_h}^f R_{k L}^b R_{00}^b, \\ (B_{UY})_{k, ph} &= (B_{XV})_{ph, k}, \\ (B_{UV})_{k, k'} &= \frac{g N_b}{4\pi} (-1)^L \int dr r^2 R_{k L}^b R_{k' L}^b R_{00}^b R_{00}^b, \end{aligned} \quad (17)$$

with $\hat{l} = \sqrt{2l+1}$. In Eq. (17) $R_{nl}^b(r)$ and $R_{nl}^f(r)$ are the radial parts of the single-particle wave functions ϕ and ψ , which are defined by $\phi_{nlm}(\vec{r}) = R_{nl}^b(r) Y_{lm}(\theta, \varphi)$ and $\psi_{nlm}(\vec{r})$

$=R_{nl}^f(r)Y_{lm}(\theta,\varphi)$ where $Y_{lm}(\theta,\varphi)$ are the spherical harmonics. We omitted $O(N_b^{-1})$ terms in this calculation. Actually we obtain the same set of equations if we replace b_0^\dagger, b_0 in Eq. (12) with $\sqrt{N_b}$, which is equivalent to the Bogoliubov–de Gennes equation for the bosonic system.

The response of the system to an external field is represented by the transition matrix elements of the relevant operators which connect the ground state and an excited state. The external probe for a collective oscillation is assumed to be long ranged and is given by the standard multipole operators, i.e.,

$$F_L(\vec{r}) = \begin{cases} \frac{1}{\sqrt{4\pi}}r^2 & (L=0), \\ r^L Y_{L0}(\theta) & (L \neq 0). \end{cases} \quad (18)$$

As the system is composed of two kinds of particle, we define operators

$$F_L^b = \int d^3r \hat{\phi}^\dagger(\vec{r}) F_L(\vec{r}) \hat{\phi}(\vec{r}),$$

$$F_L^f = \int d^3r \hat{\psi}^\dagger(\vec{r}) F_L(\vec{r}) \hat{\psi}(\vec{r}), \quad (19)$$

and their combination

$$F_L^\pm = F_L^f \pm F_L^b, \quad (20)$$

where F_L^τ with $\tau=f, b, +, -$ are respectively called ‘‘fermionic,’’ ‘‘bosonic,’’ ‘‘in-phase,’’ and ‘‘out-of-phase’’ type operators. The transition amplitudes for these operators are calculated in the RPA as

$$\begin{aligned} \langle 0|F_L^\pm|\nu L0\rangle &= \langle 0|[F_L^\pm, \mathcal{Q}_{\nu L0}^\dagger]|0\rangle \\ &= \langle 0|[F_L^f, F_{\nu L0}^\dagger]|0\rangle \pm \langle 0|[F_L^b, B_{\nu L0}^\dagger]|0\rangle, \end{aligned} \quad (21)$$

$$\begin{aligned} \langle 0|[F_L^f, F_{\nu L0}^\dagger]|0\rangle &= \sum_{ph} \frac{1}{\sqrt{4\pi}} \frac{\hat{l}_p \hat{l}_h}{\hat{L}} \langle l_p 0 l_h 0 | L0 \rangle [(-1)^{l_h} X_{phL}^\nu \\ &+ (-1)^{l_p} Y_{phL}^\nu] \int dr r^2 R_{hl_h}^f r^\lambda R_{pl_p}^f, \end{aligned} \quad (22)$$

$$\begin{aligned} \langle 0|[F_L^b, B_{\nu L0}^\dagger]|0\rangle &= \sum_k \frac{\sqrt{N_b}}{\sqrt{4\pi}} [U_{phL}^\nu + (-1)^L V_{phL}^\nu] \int dr r^2 R_{kL}^b r^\lambda R_{00}^b, \end{aligned} \quad (23)$$

where $\lambda=2$ for $L=0$ and $\lambda=L$ for $L \neq 0$. The strength distribution for the multipole operator F_L^τ is then given by

$$\sum_\nu \delta(\Omega - \Omega_\nu) |\langle 0|F_L^\tau|\nu L0\rangle|^2 \quad (\tau=f, b, +, -). \quad (24)$$

They measure the collectivity of the excited states with respect to the multipole operator which characterizes the shape (or volume for $L=0$) oscillation of the system.

More detailed information on the structure of the collective excitation may well be represented by the transition densities [25]

$$\langle 0|\hat{\rho}^\tau(\vec{r})|\nu LM\rangle = \delta\rho_{\nu L}^\tau(r) Y_{LM}(\theta, \varphi) \quad (\tau=f, b), \quad (25)$$

$$\begin{aligned} \delta\rho_{\nu L}^f(r) &= \sum_{ph} \frac{1}{\sqrt{4\pi}} \frac{\hat{l}_p \hat{l}_h}{\hat{L}} \langle l_p 0 l_h 0 | L0 \rangle \\ &\times [(-1)^{l_h} X_{phL}^\nu + (-1)^{l_p} Y_{phL}^\nu] R_{hl_h}^f R_{pl_p}^f, \end{aligned} \quad (26)$$

$$\delta\rho_{\nu L}^b(r) = \sum_k \frac{\sqrt{N_b}}{\sqrt{4\pi}} [U_{phL}^\nu + (-1)^L V_{phL}^\nu] R_{kL}^b R_{00}^b, \quad (27)$$

where $\hat{\rho}^f(\vec{r})$ and $\hat{\rho}^b(\vec{r})$ are the fermion and boson density operators,

$$\hat{\rho}^f(\vec{r}) = \hat{\psi}^\dagger(\vec{r}) \hat{\psi}(\vec{r}), \quad \hat{\rho}^b(\vec{r}) = \hat{\phi}^\dagger(\vec{r}) \hat{\phi}(\vec{r}). \quad (28)$$

Recent development of two-photon Bragg spectroscopy [22] allows us to obtain dynamical structure factors (response function) for the excitations in trapped atomic gases. They are related to the transition densities as

$$S_L^\tau(q, \Omega) = \sum_\nu |\mathcal{F}_{\nu L}^\tau(q)|^2 \delta(\Omega - \Omega_\nu), \quad (29)$$

$$\mathcal{F}_{\nu L}^\tau(q) = \int dr r^2 j_L(qr/\hbar) \delta\rho_{\nu L}^\tau(r), \quad (30)$$

where q denotes momentum transferred to the system and $j_L(qr/\hbar)$ are spherical Bessel functions of order L . The long wavelength limit of the dynamical structure factor is proportional to the strength distribution for the multipole operators defined above.

III. CALCULATION

A. Numerical procedure

We consider a boson-fermion mixture of potassium isotopes, i.e., ^{41}K (boson) and ^{40}K (fermion). We take the same value $m=0.649 \times 10^{-25}$ kg for the boson and the fermion masses. The boson-boson interaction strength g is obtained from the scattering length $a_{bb}=15.13$ nm for ^{41}K - ^{41}K [26], while the boson-fermion interaction strength h is varied. (A negative value for the scattering length a_{bf} for ^{40}K - ^{41}K was suggested in [26], although it is not well established yet.) Both particles are assumed to be trapped in the spherical oscillator potential with the same trap frequency $\omega_0=100$ Hz. The oscillator length $\xi=\sqrt{\hbar/m\omega_0}$ is 4.03 μm for the adopted value of ω_0 .

The number of bosons is fixed at $N_b=1000$, while that of fermions is calculated in the Thomas-Fermi approximation for a fixed Fermi energy $\epsilon_F=(6 \times 1140)^{1/3} \hbar \omega_0$. The latter is

determined so that the last oscillator shell with a number of quanta $N=2n+\ell$ is given by $N_{\text{Fermi}}=17$ at $h/g=0$. This gives the number of fermions $N_f=1140$ at $h/g=0$. N_f is dependent on the boson-fermion interaction strength, and it is assumed that all the subshells given by the quantum numbers (n,ℓ) are m -closed, which gives, for instance, $N_f=1050$ at $h/g=8$ and $N_f=1227$ at $h/g=-6$ for the given value of ϵ_F .

The single-particle wave functions were obtained from the coupled Gross-Pitaevskii and Thomas-Fermi equations by expanding the wave functions in the harmonic oscillator basis for the given oscillator constant ξ . We included associated Laguerre functions L_n^α up to $n=30$ for fermions and $n=15$ for bosons.

The excitation energies and the wave functions for each multipole L are obtained by diagonalization of the RPA matrix. To construct the particle-hole basis we included single-particle states for bosons up to $n=7$ for $\ell=0$ and $n=6$ for $\ell=1,2,3$, so that seven p - h configurations are included for each $L=0,1,2,3$. For fermions, four (particle) states above the Fermi level ϵ_F and up to four (hole) states below ϵ_F have been included for each ℓ . The number of Fermi p - h configurations is 240 for monopoles, 464 for dipoles, 672 for quadrupoles, and 1124 for octupoles. The dimension of the RPA matrix is twice the sum of Bose and Fermi configurations for each multipole. The number of bose configurations is the same for the four multipoles considered in the present calculation.

B. Static properties

In the ground state the fermion density distribution is much broader than that for the boson due to Fermi pressure [9,17], although at large negative values of h/g the Bose-Fermi attraction tends to produce a larger overlap of the two kinds of particle as shown in Ref. [17]. As the Bose-Fermi interaction becomes repulsive the fermions are squeezed out from the central part. This in turn causes a smaller overlap of bosons and fermions, and thus a relatively small net effect of the interaction on the binding energy. For the present choice of parameters the fermions are distributed outside the boson "core" around $h/g \approx 7$, forming a "shell" like structure [7,8,13,17]. Note that this behavior would be changed if one adopted different values for N_f/N_b and g , which may be represented by a single parameter α introduced in Ref. [9].

The condition for the validity of the Thomas-Fermi approximation used to obtain the above fermion density distribution may be expressed in terms of the local de Broglie wave length $\lambda(r)=\hbar/p(r)$, where $p(r)=\sqrt{2m(\epsilon_F-V_{\text{eff}})}$ with fermion mean-field potential $V_{\text{eff}}(r)=\frac{1}{2}m\omega_0^2r^2+h\rho_b(r)$. With this quantity, the condition becomes [27]

$$f(r)=\left|\frac{d\lambda(r)}{dr}\right|\ll 1. \quad (31)$$

At $h/g=8$ where the fermionic potential may have a most pronounced structure, the value of $f(r)$ is $\sim 10^{-2}$ except around turning points. At the turning points, however, the fermion density produces only a negligible influence on the

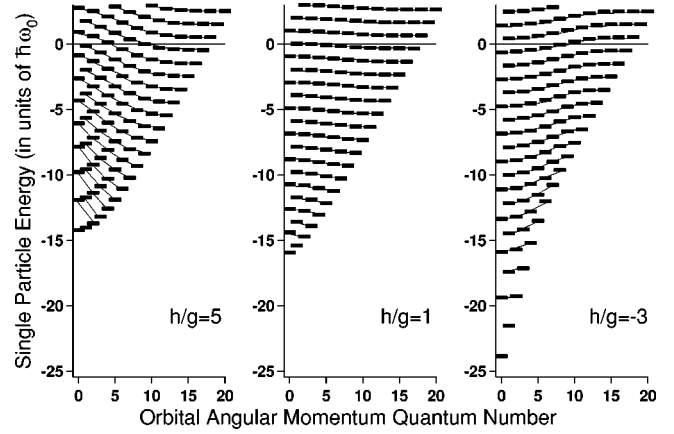


FIG. 1. Fermion single-particle energies for $h/g=5.0, 1.0, -3.0$ against orbital angular momentum quantum number. Energies are measured from the Fermi energy. Eigenstates that are degenerate at $h/g=0$ are connected by solid lines.

mean-field potential. The validity of the present Thomas-Fermi calculation may also be checked by comparing the fermion density distribution $\rho_f(r)$ obtained from Eq. (9) with the one calculated from the single-particle wave functions according to Eq. (5). The comparison of the two distribution in the range $h/g=-6$ to 8 shows that they agree within the order of 10^{-2} over the entire radial range, suggesting the consistency of the present calculation.

In Fig. 1 we show the fermion single-particle energies measured from the Fermi energy, $\epsilon_\alpha - \epsilon_F$, against orbital angular momentum ℓ for three values of the interaction parameter $h/g=5.0, 1.0, -3.0$. The Fermi energy ϵ_F is denoted by the horizontal line at zero energy. Note that ϵ_α are given by those of the harmonic oscillator at $h/g=0$, $\epsilon_{n,\ell}=(2n+\ell+3/2)\hbar\omega_0$, as we have no direct interaction among fermions. One should note also that the yrast state, i.e., the lowest state for each angular momentum, has no radial node, and the yrare one, the second lowest state, has one radial node, etc. The nodal structure of the particle and hole states around the Fermi surface is responsible for the multipole strength distribution of low-energy particle-hole excitations. The figure shows that the states with low orbital angular momentum are much influenced by the Bose-Fermi interaction, while those with high angular momentum are almost insensitive to the values of h/g . This is because the additional fermion potential due to the Bose-Fermi interaction vanishes outside the boson density distribution. For instance, since the yrast single-particle wave functions with angular momentum ℓ are peaked around $\sqrt{\ell}\xi$, those fermion states with $\ell > (R_B/\xi)^2$, R_B being a typical edge radius of the boson distribution, will not be much influenced by the Bose-Fermi interaction. (In the present case $R_B \approx 3\xi$, and the above relation gives $\ell > 9$.)

C. Energy-weighted moments and comparison with the sum rule calculation

An RPA calculation provides approximate eigenvalues and wave functions for all the individual eigenstates and is

useful to study details of the dynamics of the system. If one is interested in the gross behavior of the strength distribution or an approximate frequency of the oscillation, one may rather consider the p th energy-weighted moments of the strength distribution,

$$m_p(L, \tau) = \sum_{\nu} (\hbar\Omega_{\nu})^p |\langle 0|F_L^{\tau}|\nu\rangle|^2, \quad (32)$$

where $\hbar\Omega_{\nu}$ is the excitation energy of the state $|\nu\rangle$. These moments can be expressed as ground state expectation values of multiple commutators of F_L^{τ} with the Hamiltonian [29,30]. It is known that this relation, the sum rule, is conserved in the RPA for some of the moments, i.e., the sum in the RHS of Eq. (32) obtained from RPA eigenstates coincides with the expectation value of the commutator in the Hartree-Fock ground state [28,29]. Thus a comparison of the two would provide a criterion on the consistency of the RPA calculation. In particular, the first moment (energy-weighted sum, EWS) m_1 is calculated from the double commutator of F_L^{τ} and the Hamiltonian as

$$m_1(L, \tau) = \frac{1}{2} \langle [F_L^{\tau}, [\hat{H}, F_L^{\tau}]] \rangle_0, \quad (33)$$

where $\langle \rangle_0$ denotes a ground state expectation value [29]. We have checked that the sum rule is satisfied within 1% for all the multipole modes.

One can estimate the average frequency of the collective oscillation based on sum rules. There are several ways to define the average frequency depending on which part of the strength distribution is emphasized. In Ref. [18] the ratio of the third and the first moments

$$\bar{\omega} = \sqrt{\frac{m_3}{m_1}} \quad (34)$$

was studied based on sum rules. This definition is advantageous as it can be used to test the validity of the RPA calculation as mentioned earlier. In later discussions we consider also the average frequency calculated by

$$\omega_{av} = \frac{m_1}{m_0} \quad (35)$$

which has more weight in the low-frequency strength compared with $\bar{\omega}$. The two frequencies should coincide when a single collective state exhausts the strength. We discuss later also the width of the strength distribution defined by

$$\sigma = \left[\frac{m_2}{m_0} - \left(\frac{m_1}{m_0} \right)^2 \right]^{1/2}. \quad (36)$$

In Fig. 2 we show the average frequency Eq. (34) for $L=0,1,2$ and $\tau=+, -$ given by the sum rule (33) and the one directly calculated in the RPA. We find a good agreement of the two calculations in a wide range of the Bose-Fermi interaction parameter h for a fixed g . There is a discrepancy at very large values of $|h|$, especially in the strongly attractive case. In the latter case, an induced instability of the ground

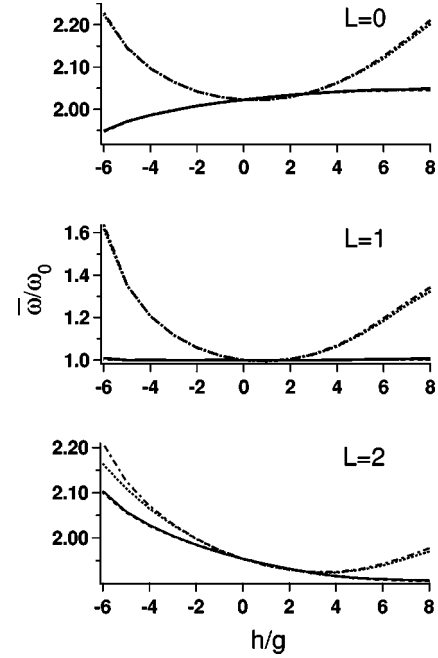


FIG. 2. Average frequencies of the collective excitations in the sum rule formalism. Average frequency $\bar{\omega}$, Eq. (34), in units of ω_0 is plotted against interaction strength ratio h/g with fixed g . Solid and dotted lines, respectively, show the in- and out-of-phase oscillations. For a comparison, average frequencies calculated from the ground state expectation values of double commutators (see Ref. [18]), are plotted by dashed (in-phase) and dot-dashed (out-of-phase) lines.

state due to the Bose-Fermi attraction may be close [16], which suggests that a larger configuration space may be required to satisfy the sum rule. In fact, by increasing the number of particle-hole states, we obtained a better agreement.

D. Distribution of multipole strengths

Now we show the distributions of the multipole strengths. Figures 3, 7, 10, and 11, respectively, show the strength distributions for $L=0,1,2$, and 3, for either the fermionic/bosonic or the in-phase/out-of-phase operators.

1. Monopole

In Fig. 3 we show the monopole strength distribution $|\langle 0|F_0^{\tau}|\nu\rangle|^2$ against Ω_{ν} , for $\tau=f,b$ and for three values of h/g . Here one expects a volume oscillation of boson and/or fermion densities. For $h=0$ and for a large number of particles, the bosonic monopole oscillation will be located around $\sqrt{5}\omega_0$ as given by the collisionless hydrodynamics [2,21], while the fermionic one is concentrated at $2\omega_0$. The latter property is due to the almost degenerate values of the relevant particle-hole energies contributing to the monopole oscillation. The present calculation shows that this situation persists even for large values of h/g , although the bosonic frequency is slightly shifted. The fermionic strength is distributed over a few states around $2\omega_0$, showing that the induced Fermi-Fermi interaction via bosons is not strong enough to make a coherent superposition of the fermion

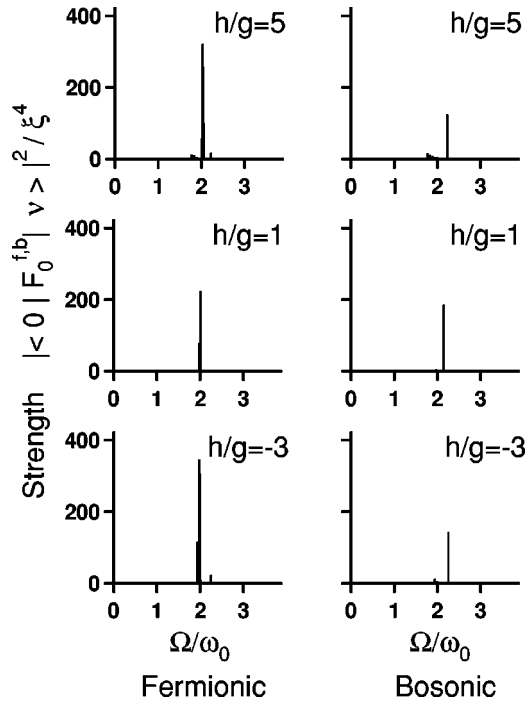


FIG. 3. Monopole strength distribution for fermionic and bosonic operators, F_0^f and F_0^b , at $h/g=5.0, 1.0$, and -3.0 . Strengths in units of ξ^4 are plotted against excitation energy.

particle-hole states. The total monopole strength for fermions is larger by an order of magnitude than that for bosons, even though the number of fermions involved in the excitation is smaller because of the Pauli principle, e.g., $m_1 = 2590\hbar\omega_0\xi^4$ for fermions and $m_1 = 419\hbar\omega_0\xi^4$ for bosons at $h/g=1$. This is because of the broader density distribution for fermions.

The strength distribution may suggest that the fermions and bosons are moving independently even for rather large values of h/g . This is not necessarily the case, however, as one may see in Fig. 4, where we plot the dynamical structure factor for the three cases, i.e., the states at $\Omega/\omega_0=2.03$ for $h/g=5.0$, at 2.01, for $h/g=1.0$ and at 1.98 for $h/g=-3.0$, which carry the largest strengths for the in-phase monopole operator. Although the fermionic strength is far larger than the bosonic one for this state, the mixture of the bosonic component is not small and is peaked at larger values of the momentum transfer q as shown by the dashed lines. The latter shows that the bosons oscillate in the inner region although this is not quite recognizable as long as one studies only the F_0 distribution.

In Refs. [16,18] we suggested that an instability toward collapse may occur at large negative values of h/g and may be signaled by the lowering of $\bar{\omega}$. In the present calculation with a smaller number of particles this is not apparent in Fig. 2. In Fig. 5 we show the strength distribution at $h/g=-6.65$. This value is close to the critical value of instability around -6.7 estimated from Mølmer's condition [7,16] and around -6.8 from the condition of Roth and Feldmeier [17]. We find a lowering of a single state which carries 13.9% of the EWS. The average frequency for this case is $\bar{\omega}$

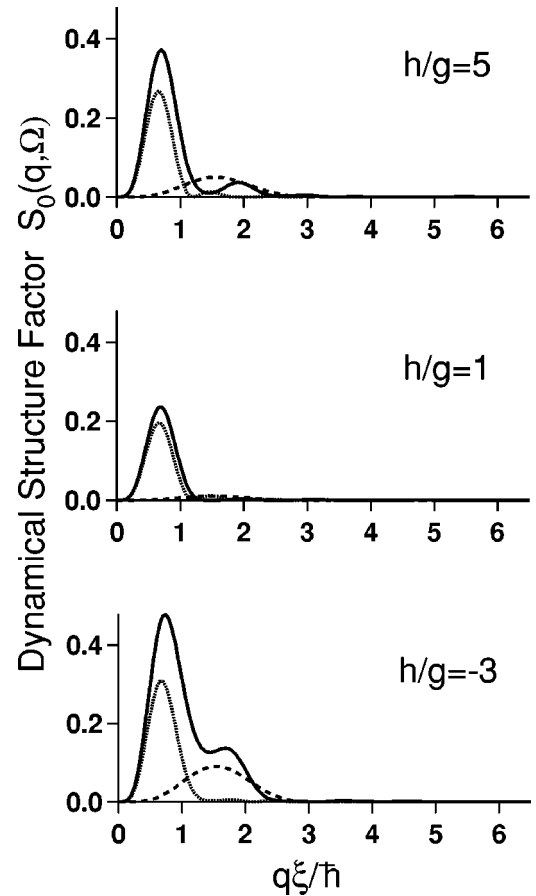


FIG. 4. Dynamical structure factors for the states in which in-phase monopole strengths are the largest. These states correspond to the ones at $\Omega/\omega_0=2.03$ for $h/g=5.0$, at 2.01 for $h/g=1.0$, and at 1.98 for $h/g=-3.0$. Dotted and dashed lines correspond to the fermion and boson transition densities $\delta\rho_{\nu 0}^{f,b}$, while solid lines are for the in-phase one, $\delta\rho_{\nu 0}^+ = \delta\rho_{\nu 0}^f + \delta\rho_{\nu 0}^b$. The abscissa is $q\xi/\hbar$, where q denotes the momentum transferred to the system by external probes.

$=1.92\omega_0$, appreciably lower than the value $\sim 2\omega_0$ for $h/g = -5$ to 5. At more negative values of h/g we could not find a stable ground state.

Let us study the character of the low-lying excited states by considering the response to the probe

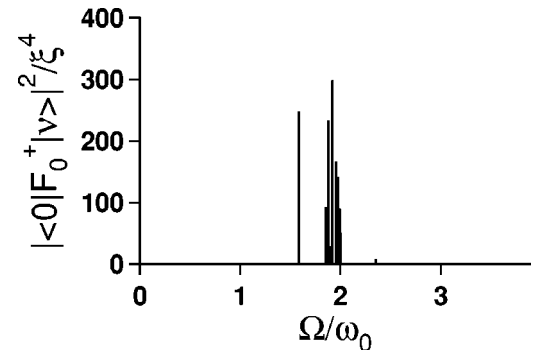


FIG. 5. Strength distribution for the in-phase monopole operator F_0^+ at $h/g=-6.65$ plotted against Ω/ω_0 .

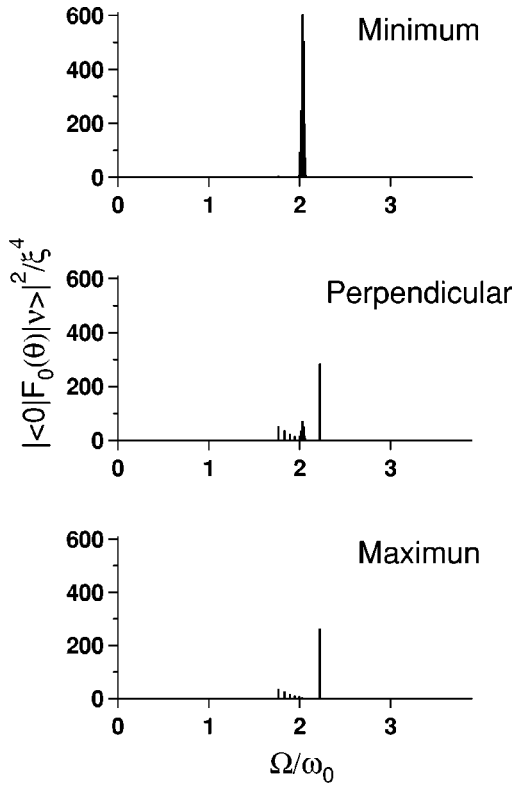


FIG. 6. Strength distribution for the θ -dependent monopole operator $F_0(\theta)$ at $h/g=5.0$. Top figure shows the strength distribution for the operator $F(\theta_{\min}=-0.12\pi)$ which was determined so as to minimize the average frequency $\bar{\omega}$. Middle figure is the one for the operator $F_{\perp}=F(\theta=0.38\pi)$ which is perpendicular to the above operator. Bottom figure is the strength distribution for the operator $F(\theta_{\max}=0.27\pi)$ which was determined to maximize the average energy.

$$F(\theta) = F^+ \cos \theta + F^- \sin \theta \quad (37)$$

parametrized by θ . In Ref. [18] the angle θ was determined by minimizing the average frequency $\bar{\omega}$ for $F(\theta)$ so as to find the character of the probe which favors the low-lying states. Once the value of the parameter, θ_{\min} , is determined for a given h/g , one may consider an operator “perpendicular” to $F(\theta_{\min})$, i.e., $F_{\perp}=F^+ \sin \theta_{\min}-F^- \cos \theta_{\min}$, which may favor the high-lying state. Alternatively, one may maximize the EWS within the model space to determine the value θ_{\max} of the operator to characterize the high-lying states. Figure 6 shows the strength distribution for these three types of operator at $h/g=5.0$. The value $\theta_{\min}=-0.12\pi$ suggests that, in this highly repulsive value of the interaction, a slightly in-phase type oscillation is favored in order to avoid an overlap of bosons and fermions (see the density distribution in Refs. [7,8,13,17]). We note that the distribution for the “perpendicular” operator F_{\perp} is concentrated and is similar to the one for $F(\theta_{\max})$. The latter, however, is an almost bosonic type operator and suggests that the strength distribution alone is not sufficient to characterize the structure of high-lying states. A similar study has been made for a very attractive case $h/g=-6.65$. In this case we obtain $\theta_{\min}=-0.01\pi$, i.e., almost in phase, and the strength distribution is

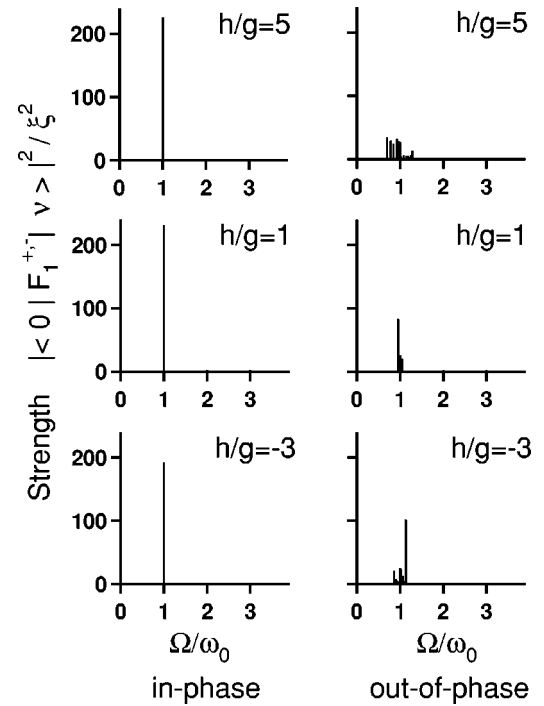


FIG. 7. Dipole strength distribution for in- and out-of-phase operators F_1^+ and F_1^- . Strengths are measured in units of ξ^2 .

similar to Fig. 5. Thus the in-phase character of the low-lying mode that favors the overlap of the two kinds of particles is clearly seen in the determination of $F(\theta_{\min})$.

2. Dipole

Dipole strength distributions for the in-phase and out-of-phase operators are shown in Fig. 7. The strong peak in the in-phase strength distribution corresponds to the center-of-mass oscillation of the whole system. For many-particle systems confined in a common oscillator potential the center-of-mass motion is decoupled from other (intrinsic) degrees of freedom of the system, resulting in an oscillation with the same frequency ω_0 . This relation can be represented by the commutation relation of the dipole operator and the Hamiltonian, and should hold also within the RPA [28]. In the present numerical calculation, however, the state at $\Omega=\omega_0$ does not exhaust the whole strength for the in-phase oscillation; the largest deviation occurs at $h/g=-1$ having 80% of the EWS. This is because the single-particle model space in our numerical calculation is not sufficient to completely decouple the center-of-mass motion, especially in strong coupling cases where the deviation of the single-particle potential from the oscillator becomes large. The m_1 sum rule is, nevertheless, almost satisfied as mentioned earlier, and is determined by the total number of Bose and Fermi particles, where the latter number is dependent on the value of h/g . A smaller value of the sum rule percentage at $h/g=-1$ is mainly due to the appearance of the almost degenerate state ($\Delta\omega/\omega_0 \approx 10^{-5}$) at this energy.

All other dipole oscillations should be orthogonal to the center-of-mass motion and thus are out-of-phase type in character. One may note that at repulsive values of h the

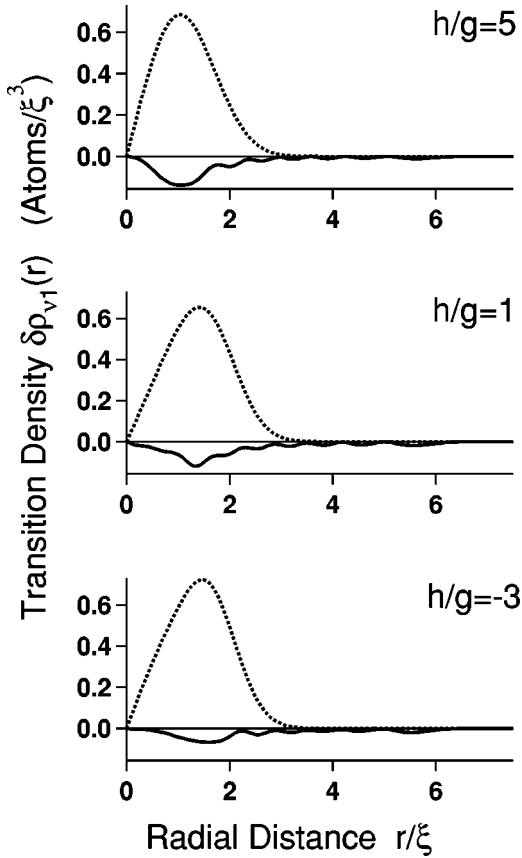


FIG. 8. Transition densities for the dipole oscillations with largest strengths of the out-of-phase type. Excitation energies of these states are $\Omega/\omega_0=0.700$ for $h/g=5.0$, 0.956 for $h/g=1.0$, and 1.14 for $h/g=-3.0$. Solid and dotted lines, respectively, show the fermionic and bosonic transition densities $\delta\rho_{\nu 1}^{f,b}$ in units of ξ^3 .

dominant part of the out-of-phase strength is located below ω_0 , although the strength carried by each individual state is not very large. As discussed in Ref. [18], this may reflect the ground state density distribution which favors the out-of-phase oscillation by making the overlap of boson and fermion distributions smaller. Figure 8 shows transition densities for the out-of-phase type oscillations at $h/g=5.0, 1.0, -3.0$ which carry the largest strengths: $\Omega/\omega_0=0.700$ for $h/g=5.0, 0.956$ for $h/g=1.0$, and 1.14 for $h/g=-3.0$. Bosons and fermions move in the opposite directions so as to make the overlap smaller around the surface of the boson distribution. One can observe that the bosonic transition density is large and robust, while the fermionic one is feeble and is spread over the whole system. This situation may be analogous to the soft dipole mode speculated to exist in neutron-rich nuclei wherein the protons oscillate almost freely in the sea of neutrons [31]. Dynamical structure factors corresponding to these states are shown in Fig. 9. Here the bosonic and fermionic responses are shown together with the one for a hypothetical out-of-phase type probe. By changing the momentum transfer one would find a structure corresponding to the oscillation of the two kinds of particle.

It was suggested in [7,19] that for a very strong repulsion between bosons and fermions with sufficient numbers of particles the system may become unstable toward a phase separation

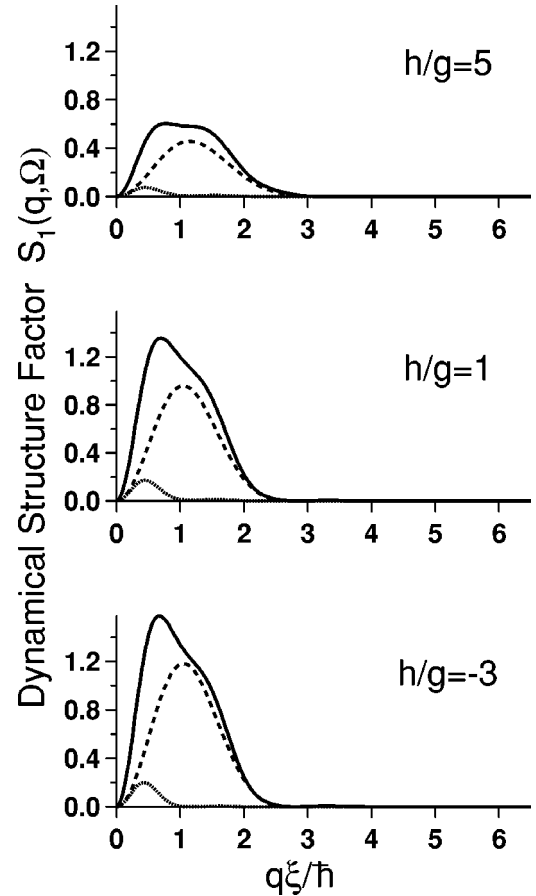


FIG. 9. Dynamical structure factors for the same states as given in Fig. 8. Dotted and dashed lines are those for the fermionic and bosonic transition densities while solid lines are those for the out-of-phase one, $\delta\rho_{\nu 1}^- = \delta\rho_{\nu 1}^f - \delta\rho_{\nu 1}^b$.

of the two kinds of particles. The out-of-phase dipole strength distribution in Fig. 7 indeed show a softening of the strength distribution at large values of h/g . We cannot conclude from the present calculation, however, whether this tendency is related to the mentioned instability.

3. Quadrupole

One finds from the quadrupole strength distribution in Fig. 10 that the fermionic strength is split into low- and high-energy parts, while the bosonic strength is concentrated. The higher strengths for the fermions are due to the $2\hbar\omega_0$ excitation of the particle from the occupied single-particle states and are similar in character to the bosonic excitation. In contrast, the lower fermion strengths come from the matrix elements of the quadrupole operator F_2 which reorient the single-particle states within the same oscillator shell of $N=2n+\ell$ around the Fermi surface. This transition normally involves a change of nodes by 1 (see Fig. 1), and the corresponding strengths are smaller than the higher ones. One may note that the quadrupole bosonic strength is located slightly higher than $\sqrt{2}\omega_0$ as expected for the collective oscillation in the large N limit [2], which may be due to the rather small number of particles in the present calculation.

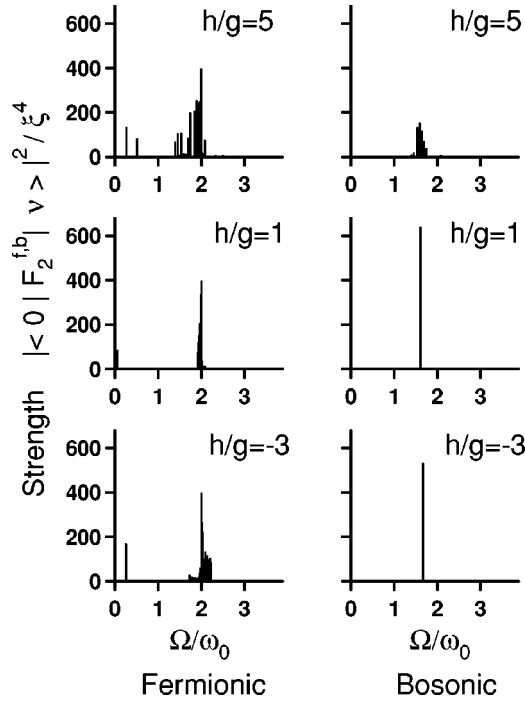


FIG. 10. Quadrupole strength distributions for fermionic and bosonic operators F_2^f and F_2^b at $h/g = 5.0, 1.0,$ and -3.0 .

We note that the strength distribution tends to be fragmented at large (repulsive) values of the interaction parameter h/g as seen in Fig. 10. This is because the average potential deviates appreciably from the harmonic oscillator potential, giving rise to a dispersion in the fermion particle-hole energies (see Fig. 1). The strong fermion-boson interaction would then be responsible for scattering the bosonic strengths, too.

4. Octupole

The octupole strength distribution is shown in Fig. 11. Here again the fermionic strength is split into $\hbar\omega_0$ and $3\hbar\omega_0$ regions due to the character of the multipole operator F_3 . We note also that the frequency of the bosonic oscillation is much larger than the hydrodynamic value $\sqrt{3}\omega_0$ [21].

We find a striking change in the fermionic strength distributions depending on the sign of the Bose-Fermi interaction. While for a strongly repulsive case ($h/g = 5.0$) the region between the low- and high-lying states is almost filled up by small strengths, the one for a strongly attractive case ($h/g = -3.0$) shows a large gap in the strength distribution. This may be traced back to the structure of the single-particle states in Fig. 1. The large strengths around $3\omega_0$ are due to high orbital angular momentum states with $\ell_p - \ell_h = 3$ which stay robust against h/g as discussed earlier. Smaller strengths due to low ℓ_p and ℓ_h states are, on the other hand, sensitive to the interaction, and the corresponding particle-hole energies are below (for $h/g > 0$) or above (for $h/g < 0$) the unperturbed value $3\omega_0$. This may be understood by noting that the particles passing through the center (small ℓ orbit) experience shallow (for $h/g > 0$) or deep (for $h/g < 0$) potentials and are thus easier or harder to excite. For the strengths

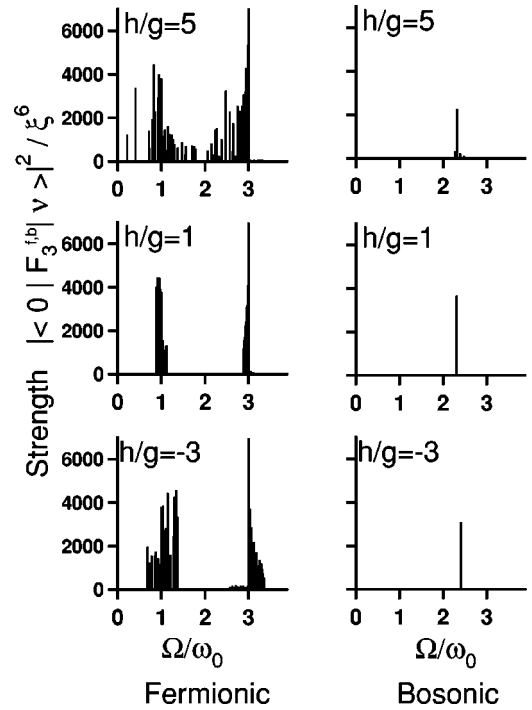


FIG. 11. Octupole strength distributions for fermionic and bosonic operators F_3^f and F_3^b at $h/g = 5.0, 1.0,$ and -3.0 .

around ω_0 different combinations of orbits are involved, and the strengths are broadened by the deviation from the oscillator potential.

E. Time evolution

To study the collective oscillation of cold atomic gases, the current experiments on BEC exert a time-dependent field on the system and then observe the time development of the shape and the size of the condensate [1]. This procedure generally excites a number of normal modes, and one may in principle be able to resolve each mode by performing a Fourier transform as long as the time duration is long enough. To simulate the situation we consider a time evolution of the system after one applies an external weak pulse of the step-function type, i.e., $\Delta V \propto F_L^\tau$ for $-\Delta t \leq t \leq 0$. The calculation is performed within the lowest-order perturbation theory. (Δt is chosen as $\Delta t = 10^{-2}\omega_0^{-1}$.)

1. Monopole

First we consider a perturbation of monopole type,

$$\Delta V = m\omega_0\Delta\omega\sqrt{4\pi}F_0^\tau \quad (38)$$

with $\Delta\omega \ll \omega_0$, which is applied to the ground state of the system for a short period Δt . The effective frequency of the external oscillator potential for fermions and/or bosons is then changed into $\omega_0 \pm \Delta\omega$ depending on the choice of τ . The time dependence of the rms radius of bosons and fermions is plotted in Fig. 12 at $h/g = -3$ for the fermionic external field $\tau = f$. The frequency of the short period oscillation is related to the average frequency of the strength distribu-

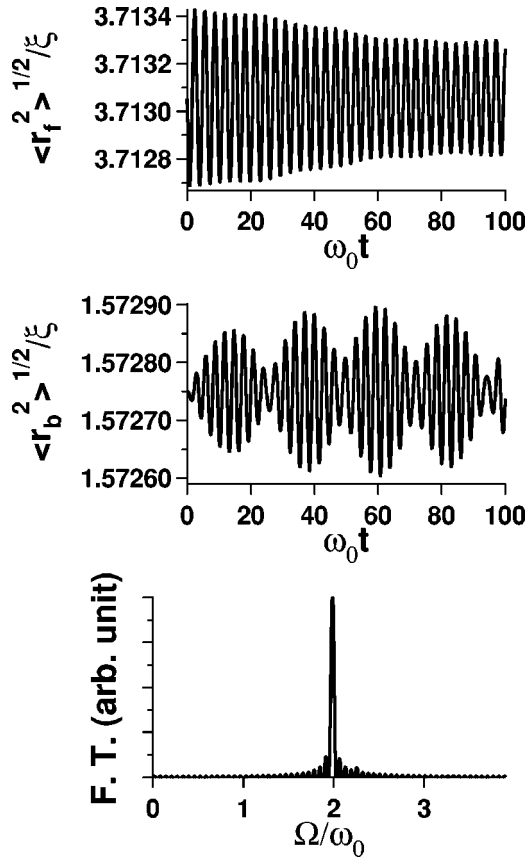


FIG. 12. Time-dependent oscillation of the Bose-Fermi system at $h/g = -3.0$ after an external impulse of fermionic monopole type, Eq. (38). Time dependences of the root-mean-square radii (in units of ξ) of fermions (upper figure) and of bosons (middle figure) are shown. Parameters of the impulse are $\Delta\omega/\omega_0 = 0.01$ and $\omega_0\Delta t = 0.01$. The differential equation in time is solved with the time mesh of $0.05\omega_0^{-1}$ up to $t_{\max} = 100/\omega_0$. The lowest figure shows the Fourier transform (in arbitrary units) of the fermionic rms radius deviation from the ground state, $\langle r_f^2 \rangle(t) - \langle r_f^2 \rangle_0$, which corresponds to the fermionic strength distribution given in Fig. 3 at $h/g = -3.0$.

tion, e.g., $\omega_{av} = 1.99\omega_0$. That of the long period one, on the other hand, reflects the width of the distribution. For instance, the slow decrease of the envelope for $\sqrt{\langle r_f^2 \rangle}$ would imply a very narrow width of the strength distribution. The bottom of Fig. 12 shows the Fourier transform of $\langle r_f^2 \rangle(t) - \langle r_f^2 \rangle_0$ which recovers the sharp peak structure of the strength distribution in Fig. 3. The time evolution of the bosonic radius shows a rather regular modulation, and its beat frequency is estimated at about $0.125\omega_0$, which is consistent with the half-width $\sigma/2 = 0.127\omega_0$.

2. Dipole

For the dipole case we take the perturbing potential

$$\Delta V = -m\omega_0^2\Delta z \sqrt{\frac{4\pi}{3}} F_1^T, \quad (39)$$

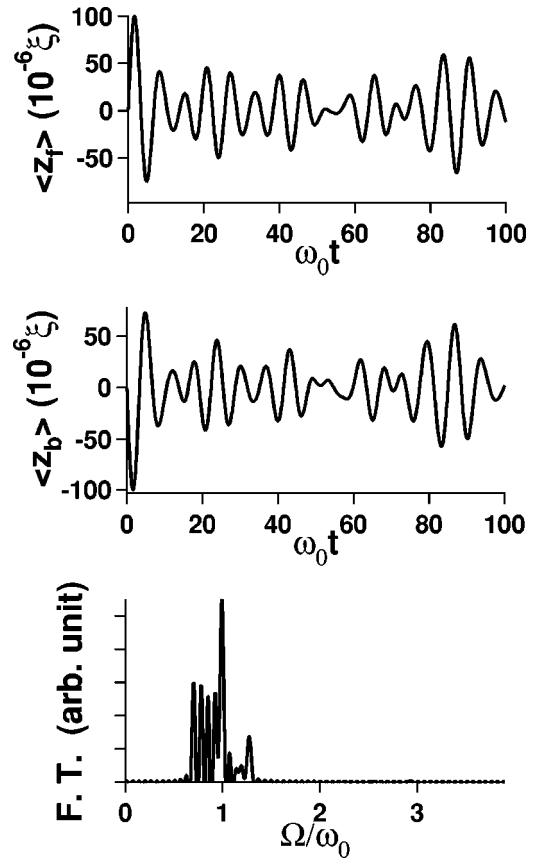


FIG. 13. Time dependence of the oscillations of fermions and bosons at $h/g = 5.0$ for an out-of-phase type external dipole impulse, Eq. (39). Top and middle figures show the fermion and boson centers of mass in units of ξ against elapsed time in units of ω_0^{-1} . Parameters are given by $\Delta z/\xi = 0.01$ and $\omega_0\Delta t = 0.01$. Calculation is performed with time mesh of $0.05\omega_0^{-1}$ and up to $t_{\max} = 100/\omega_0$. The lowest figure shows the Fourier transform (in arbitrary units) of the relative distance of fermions and bosons, $N_f\langle z_f \rangle - N_b\langle z_b \rangle$, with an energy resolution of $\sim 10^{-2}$. The figure corresponds to the strength distribution of the out-of-phase type in Fig. 7 at $h/g = 5.0$.

where $\Delta z (\ll \xi)$ measures the shift of the centers of the oscillator potentials experienced by fermions and/or bosons. In Fig. 13 we show the time dependence of the centers-of mass of bosons and fermions for the out-of-phase external dipole impulse $\tau = -$ at $h/g = 5$. The frequency of the oscillation is consistent with the average frequency $0.90\omega_0$ for the dipole strength distribution. The amplitude of the oscillation shows an irregular behavior, suggesting that the strength distribution does not have a simple structure. The lowest part of the figure shows the Fourier transform of the relative distance of the fermion and boson center-of-mass positions, $N_f\langle z_f \rangle - N_b\langle z_b \rangle$, which is sufficient to recover the behavior of the original strength distribution given in Fig. 7.

IV. SUMMARY AND CONCLUSION

In the present paper we performed a RPA calculation of a polarized Bose-Fermi mixed system of alkali-metal gases at zero temperature. We solved the coupled Gross-Pitaevskii-Thomas-Fermi equations to obtain the ground state for sev-

eral values of the boson-fermion interaction strength with a fixed value of the boson-boson interaction. Single-particle states of Bose and Fermi particles are calculated based on the mean field produced by the obtained ground state density. The density distribution constructed from the occupied single-particle orbits agrees well with the original one, suggesting the self-consistency of the calculation. We calculated and diagonalized the RPA matrix to obtain excitation energies and wave functions for multipoles $L = 0, 1, 2, 3$. We then calculated strength distributions for bosonic/fermionic and in-phase/out-of-phase multipole operators, and also transition densities and dynamical structure factors for some of the collective states.

We first calculated energy-weighted moments of the strengths to study the average behavior of the strength distribution. Comparison of the first moments with the sum rule predictions for $L = 0, 1, 2$ shows that the RPA configuration space is sufficient to within 1%. A glance at the monopole distribution suggests that fermions and bosons are moving rather independently for the adopted parameters, which turns

out not to be the case if we study the dynamical structure factors. We find, in fact, that the long wavelength oscillation of fermions in the surface is coupled to the internal short wavelength oscillation of bosons. For a strong attractive boson-fermion interaction, the calculation suggests a softening of in-phase monopole oscillations. We studied also the structure of the low-lying out-of-phase type dipole modes. Lowering of the energy is related to the ground state density distribution of bosons and fermions, which favors the out-of-phase oscillation. Transition densities for these modes suggest that the bosons oscillate on their way through the cloud of fermions, which is analogous to the soft dipole mode discussed in neutron-rich nuclei. We also calculated the strength distributions for quadrupole and octupole modes, and studied, in particular, the origin of the fragmentation of fermionic strengths. Finally, we considered the time-dependent behavior of the trapped Bose-Fermi system after an impulse of a multipole external field. By Fourier transforming the time-dependent oscillating behavior of the system, we could recover the gross structure of the strength distribution.

-
- [1] M.H. Anderson, J.R. Ensher, M.R. Matthews, C.E. Wieman, and E.A. Cornell, *Science* **269**, 198 (1995); K.B. Davis, M.-O. Mewes, M.R. Andrews, N.J. van Druten, D.S. Durfee, D.M. Kurn, and W. Ketterle, *Phys. Rev. Lett.* **75**, 3969 (1995).
- [2] F. Dalfovo, S. Giorgini, L.P. Pitaevskii, and S. Stringari, *Rev. Mod. Phys.* **71**, 463 (1999).
- [3] D.S. Jin, J.R. Ensher, M.R. Matthews, C.E. Wieman, and E.A. Cornell, *Phys. Rev. Lett.* **77**, 420 (1996); M.-O. Mewes, M.R. Andrews, N.J. van Druten, D.M. Kurn, D.S. Durfee, C.G. Townsend, and W. Ketterle, *ibid.* **77**, 988 (1996).
- [4] B. DeMarco and D.S. Jin, *Phys. Rev. A* **58**, 4267 (1998); *Science* **285**, 1703 (1999); B. DeMarco, S.B. Papp, and D.S. Jin, *Phys. Rev. Lett.* **86**, 5409 (2001).
- [5] A.G. Truscott, K.E. Strecker, W.I. McAlexander, G.B. Partridge, and R.G. Hulet, *Science* **291**, 2570 (2001).
- [6] F. Schreck, L. Khaykovich, K.L. Corwin, G. Ferrari, T. Bourdel, J. Cubizolles, and C. Salomon, *Phys. Rev. Lett.* **87**, 080403 (2001).
- [7] K. Mølmer, *Phys. Rev. Lett.* **80**, 1804 (1998).
- [8] M. Amoruso, A. Minguzzi, S. Stringari, M.P. Tosi, and L. Vichi, *Eur. Phys. J. D* **4**, 261 (1998).
- [9] T. Miyakawa, K. Oda, T. Suzuki, and H. Yabu, *J. Phys. Soc. Jpn.* **69**, 2779 (2000).
- [10] M.J. Bijlsma, B.A. Heringa, and H.T.C. Stoof, *Phys. Rev. A* **61**, 053601 (2000).
- [11] L. Vichi, M. Inguscio, S. Stringari, and G. M. Tino, *Eur. Phys. J. D* **11**, 335 (2000).
- [12] L. Vichi, M. Inguscio, S. Stringari, and G.M. Tino, *J. Phys. B* **31**, L899 (1998).
- [13] N. Nygaard and K. Mølmer, *Phys. Rev. A* **59**, 2974 (1999).
- [14] X.X. Yi and C.P. Sun, *Phys. Rev. A* **64**, 043608 (2001).
- [15] L. Viverit, C.J. Pethick, and H. Smith, *Phys. Rev. A* **61**, 053605 (2000).
- [16] T. Miyakawa, T. Suzuki, and H. Yabu, *Phys. Rev. A* **64**, 033611 (2001).
- [17] R. Roth and H. Feldmeier, *Phys. Rev. A* **65**, 021603(R) (2002).
- [18] T. Miyakawa, T. Suzuki, and H. Yabu, *Phys. Rev. A* **62**, 063613 (2000).
- [19] A. Minguzzi and M.P. Tosi, *Phys. Lett. A* **268**, 142 (2000).
- [20] P. Capuzzi and E.S. Hernández, *Phys. Rev. A* **64**, 043607 (2001).
- [21] S. Stringari, *Phys. Rev. Lett.* **77**, 2360 (1996).
- [22] J. Stenger, S. Inouye, A.P. Chikkatur, D.M. Stamper-Kurn, D.E. Pritchard, and W. Ketterle, *Phys. Rev. Lett.* **82**, 4569 (1999); D.M. Stamper-Kurn, A.P. Chikkatur, A. Gorlitz, S. Inouye, S. Gupta, D.E. Pritchard, and W. Ketterle, *ibid.* **83**, 2876 (1999).
- [23] F. Zambelli, L. Pitaevskii, D.M. Stamper-Kurn, and S. Stringari, *Phys. Rev. A* **61**, 063608 (2000); A. Brunello, F. Dalfovo, L. Pitaevskii, S. Stringari, and F. Zambelli, *ibid.* **64**, 063614 (2001).
- [24] P. Ring and P. Schuck, *The Nuclear Many-Body Problem* (Springer-Verlag, New York, 1980).
- [25] F.E. Serr, T.S. Dumitrescu, T. Suzuki, and C.H. Dasso, *Nucl. Phys. A* **404**, 359 (1983).
- [26] R. Coté, A. Dalgarno, H. Wang, and W.C. Stwalley, *Phys. Rev. A* **57**, R4118 (1998).
- [27] L. D. Landau and E. M. Lifshitz, *Quantum Mechanics Non-Relativistic Theory*, 3rd ed. (Butterworth-Heinemann, Oxford, 1981).
- [28] D. Thouless, *Nucl. Phys.* **22**, 78 (1961).
- [29] O. Bohigas, A.M. Lane, and J. Martorell, *Phys. Rep.* **51**, 267 (1979).
- [30] E. Lipparini and S. Stringari, *Phys. Rep.* **175**, 103 (1989).
- [31] K. Ikeda, *Nucl. Phys. A* **538**, 355c (1992).